*Indian J. Phys.* **71B** (3), 393–414 (1997)

**IJP B**
— an international journal

# Elastic and inelastic x-ray scattering; the need for experimental and theoretical cross sections

C. J. Sparks and G. E. Ice
Oak Ridge National Laboratory
Oak Ridge, Tennessee 37831-6118, USA

**Abstract:** The development of tunable ultra-brilliant synchrotron radiation sources has created an urgent need for a more quantitative understanding of x-ray absorption, scattering and radiative process. Crystallographers interested in the structure and chemistry of matter increasingly use tunable synchrotron radiation to approach absorption edges for maximum elastic-scattering contrast between elements; large values for the x-ray dispersion terms for an element near its absorption-edge energy change the amplitude and phase of its x-ray atomic scattering factor. Although near-resonant x-ray scattering allows additional control of the elastic-scattering cross section, experiments near an absorption edge are complicated by inelastic-scattering processes and uncertainties in the absorption and index of refraction. For example, weak diffuse x-ray scattering associated with imperfect periodicity can be contaminated by inelastic radiation, which complicates the measurement of crystal defects and increases the uncertainties in the recovered parameters. The channels for inelastic scattering become particularly strong near threshold. Better understanding and quantitative cross sections for the radiation absorption process, their substantial effect on the index of refraction and the inelastic radiation generated as background to the elastic intensity will improve the crystallography of complex materials. Values of the absorption cross sections are required especially within ~ 500 eV of the edge to place intensity measurements into absolute units and correct for absorption in various sample geometries. Tabulations of inelastic-scattering (radiative) processes are also needed near threshold. Among the many inelastic channels contributing to the

inelastic-scattering background are Compton, Compton-Raman, plasmon, bremsstrahlung, radiative-Auger, and resonant-Raman scattering. Crystallographers need to understand these processes quantitatively and within a framework where cross sections can be computed and tabulated for x-ray energies near absorption edges. Here we argue the needs from the crystallographer's point of view for improved tabulated cross sections for the various elastic and inelastic-scattering processes including absorption.

Keywords: inelastic x-ray scattering, plasmon scattering, Compton scattering, radiative-Auger effect, resonant-Raman scattering, bremsstrahlung, x-ray interactions

PACS numbers: 32.80.-t, 32.80.Cy, 32.30.Rj

## 1. Dispersion and Absorption

### A. Historical introduction

A study of photon interactions near the excitation threshold of bound electrons was one of the first experiments performed with Röntgen's newly discovered x-rays [1]. With light as a model for the interaction of electromagnetic radiation with matter, similar properties were studied for x-rays. Röntgen's experiment with prisms failed to measure the very small index of refraction for x-rays. Unlike visible light which has a strong resonance with the loosely bound continuum-electron states of atoms, x-ray energies were usually removed from sharp resonances with the more tightly bound states. These resonances are reflected in the jumps of the x-ray absorption coefficients, which occur at the excitation threshold for photoionization and where rapid changes take place in the index of refraction. In the x-ray regime, the term "anomalous dispersion" or "anomalous scattering" has been widely used to describe the change in dispersion angle $d\theta$ which increased with an increase in wavelength $d\lambda$ and is just the opposite to that for visible light. Current sentiment leans towards the use of "resonant" or "dispersion" to replace anomalous.

Much attention was given to the measurement of x-ray absorption as the major early use for x-rays was for radiography of the human body. With the discovery of diffraction by von Laue and collaborators [2] and its interpreta-

tion in terms of crystallographic planes by Bragg [3], much interest was generated for the use of scattered x-rays to study the structure of matter. Initially, interest in the x-ray scattering amplitudes was motivated by curiosity in the basic physics rather than for solving crystal structures. Thomson's [4] calculation of the elastic-scattering amplitude for a free electron required a correction in the vicinity of an absorption edge because of the many bound states. Waller's [5] use of the new quantum theory for derivation of these resonant (dispersion) correction terms, the real part $f'$ and imaginary part $f''$, to Thomson's frequency independent term $f_0$ led Hönl [6] to calculate their values which he tabulated for use by crystallographers. (See Templeton [7] for this early history). The x-ray atomic scattering factor is usually written for atom j as

$$f_j(\boldsymbol{h}, E) = f_{oj}(\boldsymbol{h}) + f_j'(E) + if_j''(E) \tag{1}$$

where $|\boldsymbol{h}| = 4\pi\lambda^{-1}\sin\Theta$ ($\Theta$ is the Bragg angle equal to $\theta/2$ where $\theta$ is the scattering angle) and incident energy $E$ are the major independent variables when polarization is neglected.

X-ray energies then available for diffraction were dominated by characteristic fluorescent lines with energies not usually near-edge energies of bound electrons. Thus, the values of $f'$ and $f''$ were usually small and crystallographers were satisfied in just having reasonable values of these corrections to the x-ray atomic scattering factor $f_0$ to improve their structure determinations.

### B. Determination of real $f'$ and imaginary $f''$

The two properties of light, refraction and absorption, are related and can be calculated from each other. If we know the absorption spectrum, the imaginary resonant term $f''$ can be calculated directly from the photoelectric absorption $\mu(E_i)$ with the optical theorem [8]

$$f''(E_i) = \frac{mc\, E_i\, \mu(E_i)}{2he^2} \tag{2}$$

where $E_i$ is the incident energy, $m$ and $e$ the mass and charge of the electron, $h$ Planck's constant and $c$ the speed of light. In turn the real part of the resonant scattering is determined from $f''$ with the Kromers-Kronig [9] relationship

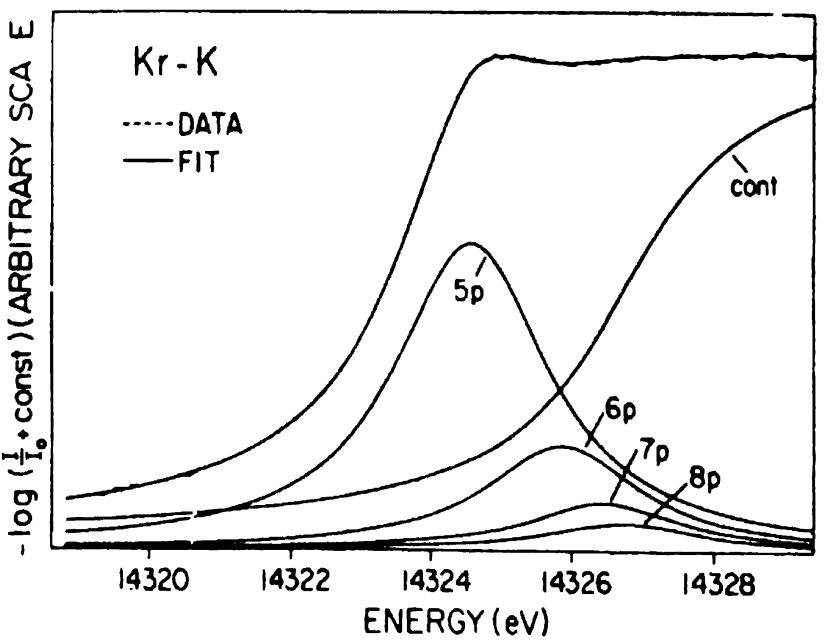


Fig. 1. K-edge absorption cross section for Kr with the contributions from various transitions shown (after Breinig et al Ref. [10]).

$$f'(E_i) = \frac{2}{\pi} \int_{E=0}^{\infty} \frac{E f''(E)}{E^2 - E_i^2} \, dE. \tag{3}$$

These relationships are derived and discussed in great detail by James [8]. A more modern treatment referred to as the S-matrix theory is discussed by Kissel in this series. However, solid-state effects on absorption are difficult to include and requires the experimentalist to measure the absorption edge of interest. A typical absorption edge such as the Kr *K* edge taken-from the work of Breinig et al. [10] is shown in Fig. 1. Here the edge is shown to consist of a series of lifetime-broadened transitions from the 1*s* state into the unfilled bound states 5*p*, 6*p*, 7*p*, 8*p* in addition to the continuum (cont). This picture differs from the one-electron model shown in Fig. 2 which ignores the Lorentizian lifetime broadening of the inner-shell hole. The effect of broadening is indicated by the dashed line in Fig. 2 as given by Ice et al. [11]. Widely used values of $f'$ and $f''$ from Cromer and Liberman [12] do not contain the effects of lifetime broadening, of pre-edge transitions to unfilled bound states

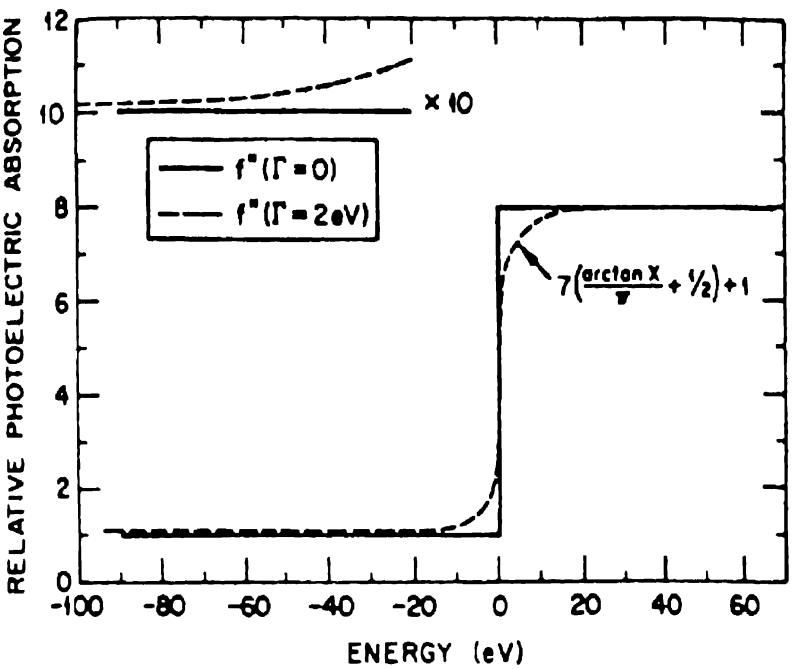


Fig. 2. The usual tabulated values of the resonant (anomalous) scattering terms are not corrected for hole width (lifetime) which causes a Lorentizian broadening of the absorption edge and affects the values of $f'$ and $f''$ near the edge. (After Ice et al. [11].)

or other x-ray absorption fine structure XAFS.

A practical method to obtain more precise resonant corrections near absorption edges is to measure the absorption edge and then normalize the data to theoretical values beyond any oscillations [13]. Even though absolute x-ray photoelectric-absorption cross sections are not known to better than 5% or with larger errors near edges [14], measured values of $f'$ and $f''$ may approach precisions of 0.2 electrons in the most favorable cases [15,16]. Theory and experiment can have even larger discrepancies [15,16] especially within 200 eV of an absorption edge.

### C. Absolute intensity calibration

In addition to the need for more precise x-ray absorption cross sections for improved values of the dispersion terms, calibration of intensity measurement in absolute units also require knowledge of the absorption process. Mea-

sured intensities in absolute units must be corrected for the absorption of radiation entering and leaving the sample. Standard scatterers, to which measured intensities are compared, are normally calibrated at but one energy and are not usually the same elemental composition as the sample [17]. These standard scatterers also correctly account for beam path transmission, and for the efficiency and solid angle of the detector. As normalization between data sets taken at multiple x-ray energies near absorption edges would greatly benefit from absorption coefficients known to 1% or even less, there is a need for more precision in their tabulated values and for inclusion of lifetime broadening. This is especially true near absorption edges where data set differences are taken to highlight different atoms. These intensity differences are used to recover pair-correlation functions for specific pairs and for phasing in crystal structure determinations [18].

## 2. Diffuse Elastic Scattering and Inelastic Background

### A. Introduction and Compton scattering from bound electrons

The existence of fine structure on the absorption-edge spectrum has been known since 1920, both theoretically [19] and experimentally [20]. The correct explanation given then was the promotion of an inner-shell electron into an unfilled bound state. Bergengren [20] was the first to demonstrate the effect of chemistry on this near-edge structure. By 1924 the effect of the chemical environment on x-ray line spectra was discovered [21]. This line spectra or characteristic fluorescent radiation and the continuous x-ray spectrum often referred to as bremsstrahlung were the common features of x-ray spectra known until 1923. In 1923 Compton observed and described the change in wavelength of x-rays scattered from free electrons [22]. This radiation would also be expected from x-rays scattering off bound electrons as predicted in 1923 by Smekal [23] and followed by Compton [24] in 1924. A report of the observation of this Smekal-Compton scattering from bound electrons was made by Davis and Mitchell in 1928 [25]. However, their observation was disputed [26]. In 1928 Raman had predicted frequency changes in the visible region corresponding to electron transitions between states for which the electron is retained in the atom [27]. DuMond advanced the use of Compton scattering as a probe of the momentum distribution of electrons [28]. Inelastic scattering from bound electrons was more clearly observed by Das Gupta in 1959 [26] with confirmation by Suzuki in 1964-67 [30]. Such scattering in the x-ray region has been referred to as Compton-Raman and Smekal-Raman scattering. An example of this x-ray Raman-type scattering from bound electrons is shown in Fig. 3. The usual Compton shift with

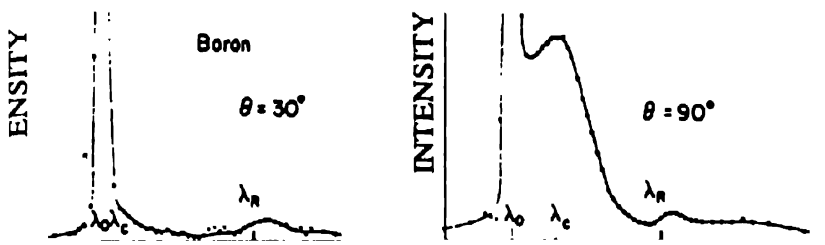


Fig. 3. X-ray inelastic scattering of $\lambda_0$ = Cr $K_\alpha$ (5412 eV) from boron at different scattering angles shows the scattering from bound *K*-shell electrons at $\lambda_R$ and the increase of the Compton shift $\lambda_C$ and intensity with momentum transfer. (After T. Suzuki et al., Ref. [31].)

momentum transfer $\lambda_C$ is taken from the work of Suzuki et al. [31] and shown with the scattering from the bound *K* electrons marked $\lambda_R$ which is fixed at an energy loss equal to the binding energy of the *K* shell of boron. The energy position of the Compton-Raman scattering from bound electrons does not shift with momentum transfer, but the intensity increases [32]. The flat intensity distribution of the *K*-shell-scattered intensity relative to the valance electrons is caused by the larger momentum distribution of inner shells compared with outer shells. This Compton-Raman scattering which shifts the incident energy down by the energy of a bound shell is a consequence of conservation of energy; an incident energy less than the binding energy is insufficient to promote the bound electron to an unoccupied state. A good review of this early period has been given by A. Pimpale and C. Mande [33]. These Compton-induced transitions of bound electrons to unfilled bound states have been reported to show absorption edge structure [34].

A major concern to crystallographers is the removal of Compton-Raman and plasmon-scattering contribution to diffuse elastic-scattering measurements. Tabulated theoretical Compton intensities [35,36] calculated with the impulse approximation are used to correct intensities measured in absolute units to obtain the elastically-scattered component. Precision of these Compton-scattering cross sections has not been well documented over the full range of momentum transfer of use to crystallographers.

## B. Plasmon dynamical scattering

Conduction in a metal represent an electron plasma of great density with about $10^{23} e^-$ per $cm^3$. This electron plasma can oscillate at eigenfrequencies which corresponds to an energy of ~ 10 to 20 eV. This is a longitudinal elec-

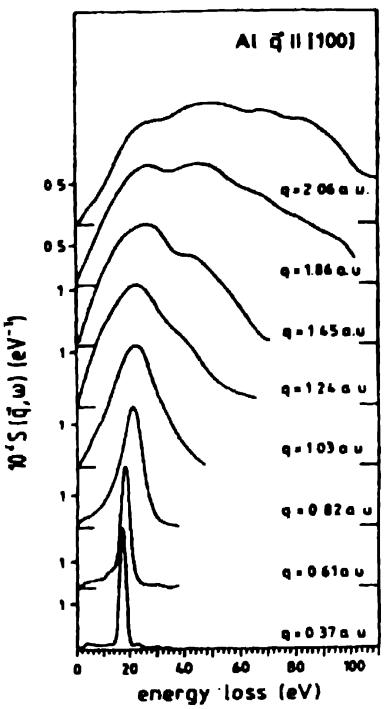


Fig. 4. Effect of momentum transfer $q = 4\pi\sin(\theta/2)/\lambda$ for 7.99-keV x-rays on the plasmon scattering from an Al single crystal. (After Shülke et al., Ref. [39].)

tron density fluctuation. The quanta of this oscillation are called plasmons. X-ray plasmon scattering has been predicted [37] and observed [38]. There has been no observed resonant behavior near the edge. The intensity increases and spreads in energy with increasing momentum transfer and becomes the usual Compton scatter. An example is shown in Fig. 4 where the sharp plasmon peak with an energy loss of ~ 20 eV at low momentum transfer gradually broadens into the classical Compton distribution as momentum transfer increases. (Various symbols are used for the momentum transfer vector; $\boldsymbol{H}$, $\boldsymbol{h}$, $\boldsymbol{Q}$, $\boldsymbol{q}$, $\boldsymbol{S}$, $\boldsymbol{K}$...) This example is taken from the work of Shülke et al. [39]. Separation of this dynamical scattering from the elastic-scattering component requires good energy resolution at low momentum transfers. The shape of the plasmon scattering is very dependent on the chemical combination of the elements.

Nearly-free-electron metals gather more of the Compton scatter into a sharp plasmon-scattering peak. Compton-scattering cross sections include the contribution from all the electrons, and therefore include the plasmon scattering but fail to give the correct distribution.

## C. Radiative-Auger effect

On the low-energy side of characteristic fluorescent lines, low-energy satellites have been attributed to a "radiative-Auger effect". Such observations were reported as early as 1935 [40]. In the radiative-Auger effect the normal fluorescence is accompanied by the simultaneous excitation of an electron into an unfilled bound state which downshifts the x-ray energy. Much recent research on this effect has shown these radiative transitions in many elements [41], and a theoretical description has been given [42]. A historical

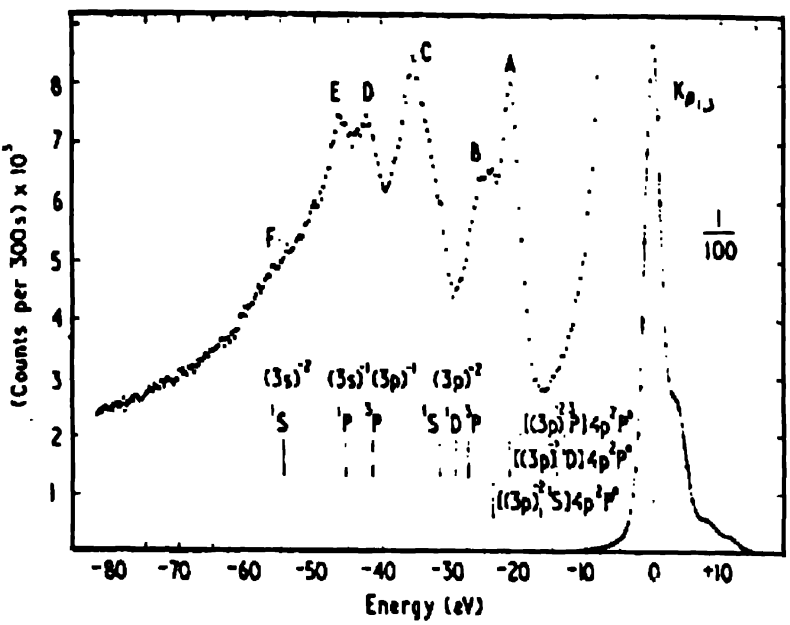


Fig. 5. Inelastic scattering on the low-energy side of the Ar $K\beta_{1,3}$ line excited by Cr $K\alpha$ and $K\beta$ radiation. (After Keski- Rahkonen and Utriainen, Ref. [44].)

review is given in Ref. [43]. When x-rays are above the threshold energy for photoionization, the ionized atom can undergo fluorescence, emit an Auger electron or with a much reduced cross section, $\sim 10^{-2}$ of the fluorescence, undergo a radiative-Auger transition. In this case an x-ray is emitted but reduced in energy from the fluorescent energy by the presence of two core holes. For example, for *K* shell ionization there could exist two *L* vacancies $K\text{-}L^2$ or *K-LL*, or two *M* vacancies, *K-MM*. The energy downshift from the *K-L* fluorescent line is more than the energy of the additional *L* hole because of the rearranged screening processes. An example for the radiative-Auger spectrum for Ar is shown in Fig. 5 [44]. On the low-energy side of the Ar $K\beta_{1,3}$ fluorescent line is the fine structure associated with the filling of a 1*s* hole by an *M* electron with another *M* electron being simultaneously excited into an unfilled bound state. The sharp features represent various electron rearrangements when an electron is promoted to an unfilled bound state. The lower-energy tail reflects the kinetic energy loss to the Auger electrons excited into the continuum state. When the incident x-ray energy is near threshold, a crystal spectrometer would be required to separate the fluorescence and radiative-Auger inelastic scattering from the elastic scattering.

### D. High-energy satellites

In addition to this scattering on the low-energy side of the characteristic fluorescent line, there is structure on the high-energy side attributed to multiple ionization where two or more electrons are simultaneously photoejected from the atom. These so-called "non-diagram" lines were first observed by Siegbahn and Stenström [45] in 1916 and explained by Wentzel [46] in 1921. More recently some of these higher-energy satellites to fluorescent lines have been shown to be associated with near-edge resonances by Deslattes et al. [47]. When the incident energy is near threshold, more than one electron can be promoted to an unfilled bound state. Several combinations exist even for double-vacancy states: 1) doubly-excited neutrals with electrons promoted to unfilled bound states, 2) excited single ions, and 3) excited double ions [47]. There are also many possible excited-state configurations for each of these combinations. It would be useful to have clear rules and simulated spectra for when high- and/or low-energy satellites would appear, especially near threshold.

### E. Bremsstrahlung radiation

We usually think of bremsstrahlung radiation as that emitted from the slowing down of electrons impinging on metal-target x-ray tubes. In addition, the slowing down of photoejected and Auger electrons can give off bremsstrahlung radiation. (See paper by Pratt in this issue for a fuller discussion of bremsstrahlung). The discovery of bremsstrahlung isochromat spectroscopy (Bis) or inverse photoemission ($XPS^{-1}$) has shown that an electron can be suddenly stopped in an unfilled bound state giving up all its kinetic energy into a single x-ray. Such studies provide a means to probe the unfilled bound states of matter [48,49].

It seems reasonable to presume that photoejected and Auger electrons could also be stopped in unfilled bound states and give all their kinetic energy to the production of x-rays. Besides the broad continuum bremsstrahlung spectrum, there would then be superimposed maxima at energies corresponding to specific photoejected and Auger electron energies. Such x-ray energies would match the energies observed for the radiative-Auger process and for Compton-Raman scattering from bound electrons as discussed earlier. There is a need for at least estimates of the cross sections for bremsstrahlung scattering from photoejected or Auger electrons. A spectrum of the Compton-Raman scattering from bound electrons is shown in Fig. 3. The leading edge of the maxima is the incident energy minus the energy of a bound electron similar to that expected for bremsstrahlung from photoejected or Auger elec-

trons captured in unfilled bound states. Several of the inelastic-scattering processes we have discussed including the following resonant-Raman scattering would produce similar spectra.

### F. Resonant-Raman scattering

When the incident energy $E_i$ is just below that of a bound electron $E_K$ (for example) there is a resonant interaction of the x-ray with the bound electron. In this case there is an emission of inelastic radiation first reported by Sparks [50,51]. An example is shown in Fig. 6. This inelastic emission of x-rays is explained by the promotion of a bound-state electron into an unfilled bound state just above the Fermi energy $E_F$ [50-53]. This process is shown schematically in Fig. 7.

Here the incident x-ray of energy $h\nu$ which is below the $K$ threshold excites those electrons in the Lorentizian tail whose lifetime broadened energy is equal to or less than $h\nu$ into unfilled bound states above the Fermi energy. When the $L$ electron fills the $K$-shell hole either x-rays or Auger electrons are emitted [54]. The emitted inelastic x-ray has an energy which is shifted down by the binding energy of the $L$ electron in this example or other lesser-bound shells which are permitted by allowed transitions.

## 3. Summary of X-Ray Interactions in Condensed Matter

### A. Primary and secondary processes

Resonant-Raman scattering like Compton-Raman from bound electrons, radiative-Auger emission and possibly bremsstrahlung from photoejected and Auger electrons produces inelastic x-rays differing in energy from the incident x-rays by the binding energies of the electrons in their single- or multiple-excited states.

With the many kinds of electron and x-ray interactions it is useful to try and build a common framework to which the details can be attached. This is illustrated in Table 1. When x-rays or electrons interact with matter they are either absorbed or scattered. If absorbed they excite the atom which then deexcites with the emission of photons or electrons. If scattered they are either elastically scattered (Raleigh scattering with no energy loss) or inelastically scattered (Raman scattering with an energy loss).

We trace these processes, as shown in Table 1 for x-rays, through their primary and secondary interactions until x-rays are reformed to start the primary processes of photoionization and scattering over again. Most of the energy deposited in the sample by the incident x-rays will eventually be con-

Table 1. Interactions of x-rays (1 to 40 keV) in condensed matter. The processes are followed through to the reformation of x-rays at which point the primary processes start over again. Most of the incident x-ray energy ends up as heat in the sample.

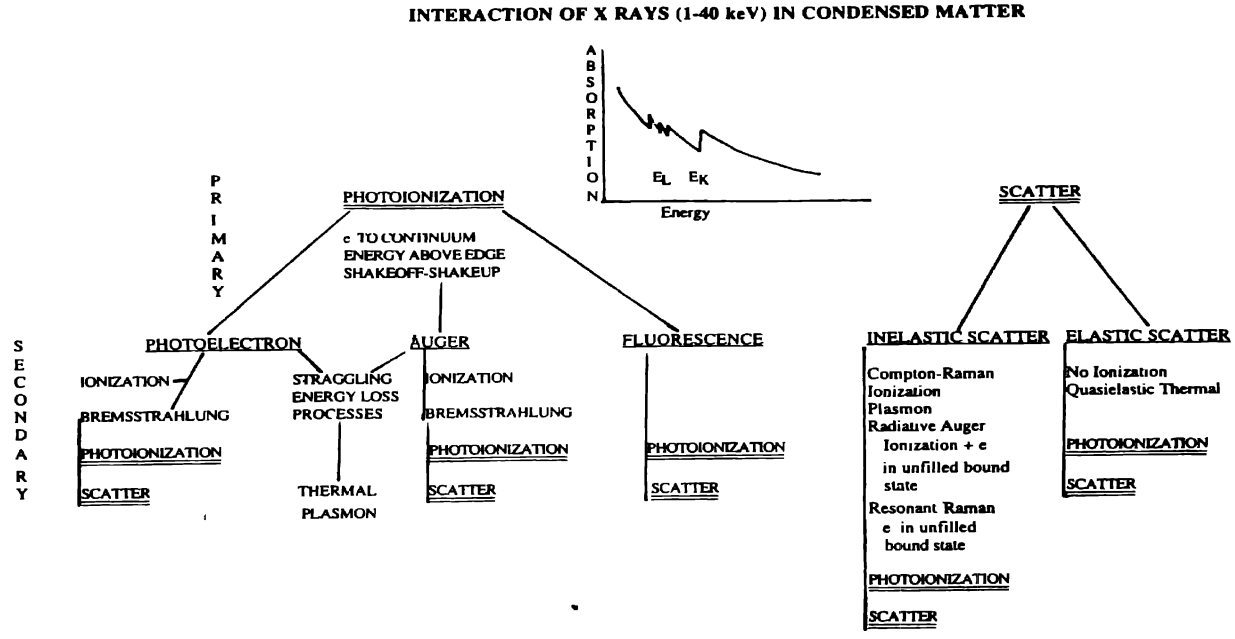

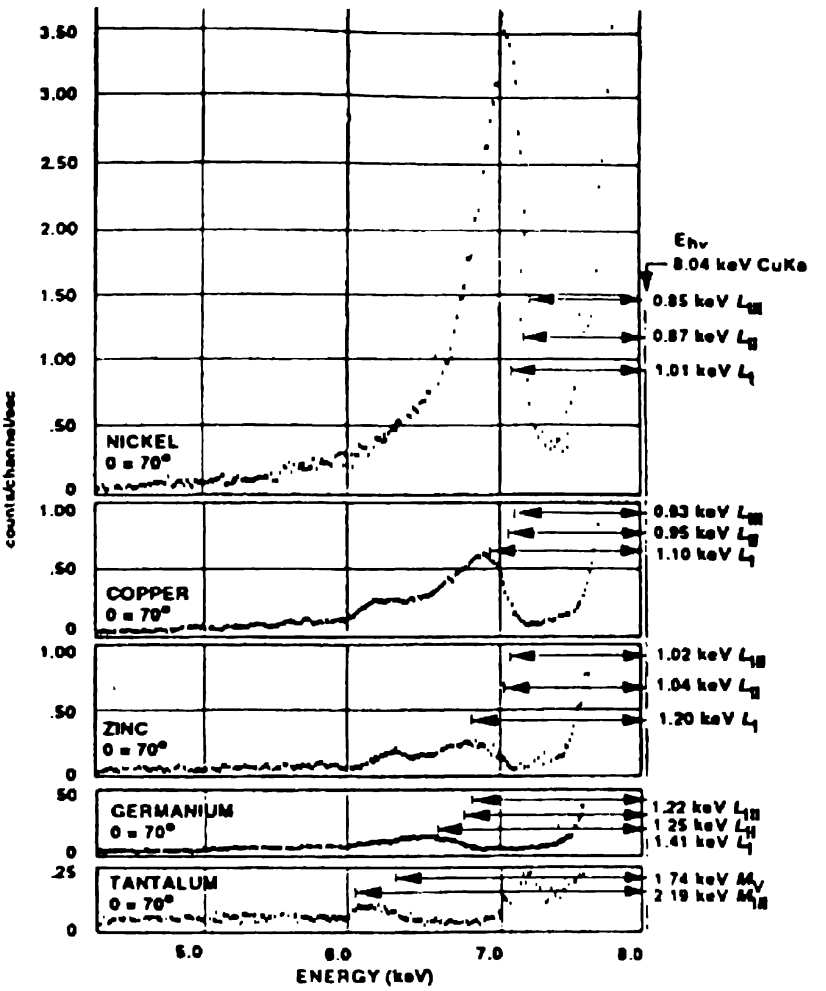


Fig. 6. An inelastically-scattered intensity excited by $E_{h\nu}$ = 8.04 keV was found to increase in resonance with the decreasing energy difference between the exciting and nearest but higher-energy bound-electron state of the sample. The energy loss is shown to be the binding energy of an $L$ or $M$ shell in these cases. (After Sparks Ref. [50].)

verted to heat by a combination of these processes. An estimate of the power spectrum as a function of incident and scattered x-ray energy for various targets would be useful for background corrections to elastic-scattering measurements.

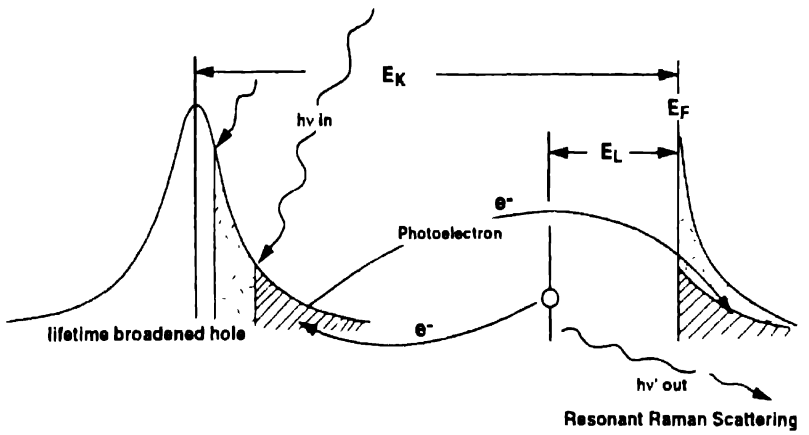


Fig. 7. Schematic for the resonant-Raman scattering process. An incident photon $h\nu$ with an energy less than that for the $K$ bound state excites electrons in the Lorentizian tail to unfilled bound states and beyond. The filling of the virtual hole by the $L$ electron creates the resonant-Raman photon $h\nu'$ with the atom left with a single vacancy in the $L$ shell. As the incident energy $h\nu$ approaches threshold, the resonant-Raman peak narrows in energy.

## B. Typical radiation spectrum

Shown in Fig. 8 is a schematic of the radiation spectrum for the processes previously discussed and including fluorescence when 8-keV x-rays strike a Cu target. In Fig. 9 the energy scale is expanded to emphasize those x-rays which are closest in energy to the incident radiation, which is elastically scattered. For elastic-Bragg scattering this inelastically-scattered radiation is a weak background easily removed by extrapolation under the Bragg peak. When the interest is in the weak diffusely-distributed intensity associated with deviations from this regular periodicity, then the inelastic background can make a significant contribution of concern to crystallographers. (See Ref. [11] and other articles in the same book on the measurement of short-range correlations.)

The removal of this inelastic radiation from the elastic spectrum requires diffracted beam spectrometers. The response of Bragg-diffraction spectrometers are sensitive to beam spread on the sample and further reduce the already weak signal [11]. An example of such a spectrum from a Fe-Ni crystal irradiated with 7092-eV x-rays (20 eV below the Fe $K$ edge) is shown in Fig. 10.

Because of the variety of useful information that x-rays and electrons bring to the study of matter, simulations of both the x-ray and electron spectra, excited by x-rays, would be useful. Such information guides the experimen-

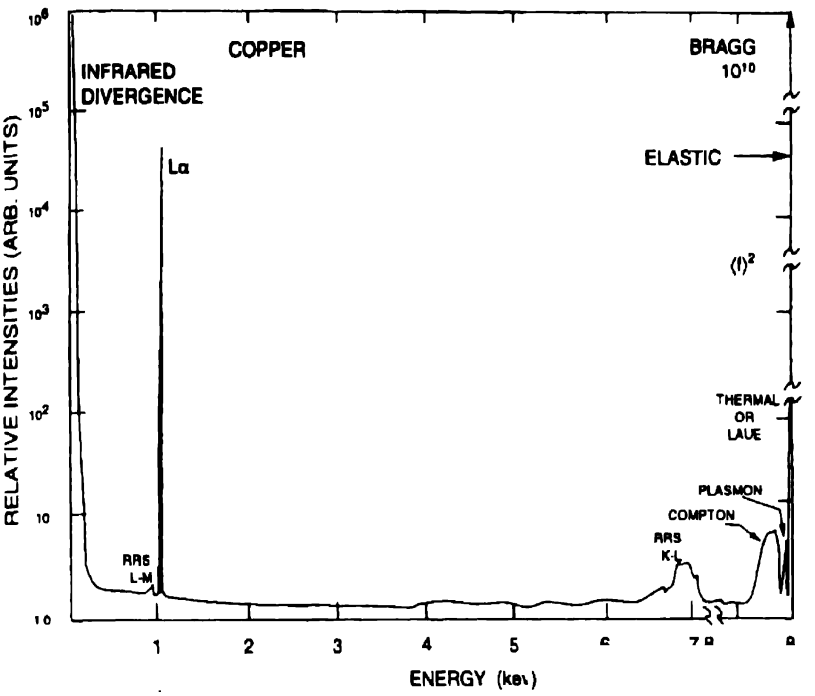


Fig. 8. Schematic of x-ray spectrum generated by 8-keV x-rays on copper.

talist in planning experiments and interpreting the data.

## 4. Summary of X-Ray Interactions and Applications

Because of the varied excitation and de-excitation channels for atoms, there are many useful spectroscopies and crystallographic applications of x-ray from interactions with matter. Table 2 is a listing of some of the more obvious information obtained from the photoionization and scattering of x-rays.

## 5. Conclusions

The resonant-dispersion corrections to the x-ray atomic scattering factors affect the diffracted intensity and are sensitive to the near-edge absorption structure through the Kromers-Kronig transform of the absorption spectrum. This near-edge structure in absorption arises from the changing transition probabilities of promoting an electron into unfilled bound states.

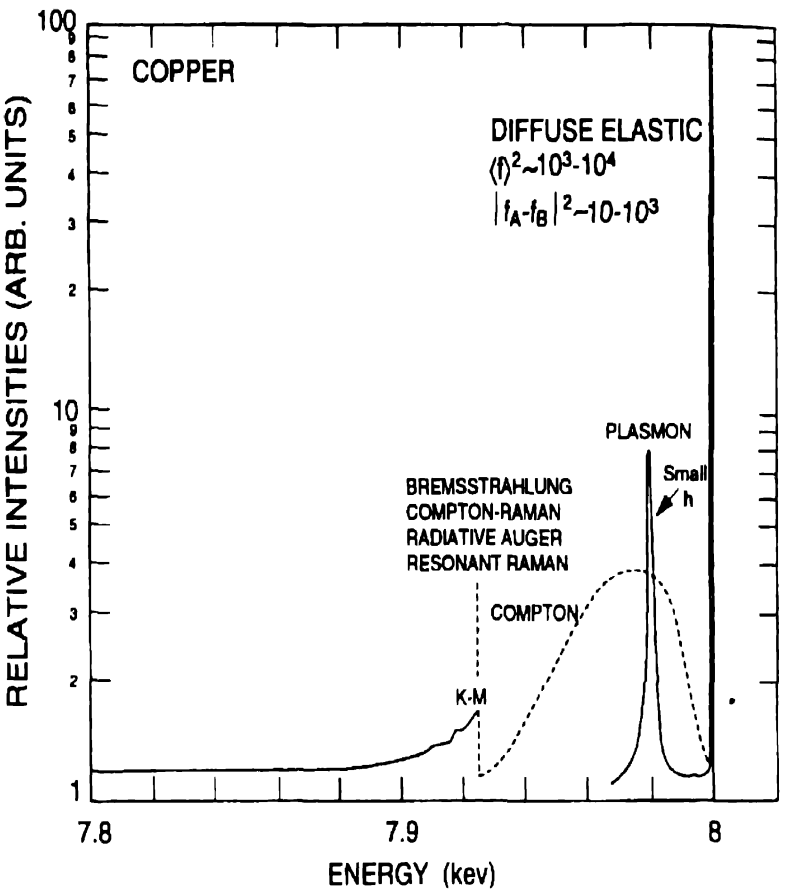


Fig. 9. Inelastic-scattering processes can place appreciable intensity near the elastically-scattered energy. Several processes result in x-rays with energies decreased by the energy of bound electrons.

These transition probabilities or oscillator strengths are polarization dependent and reflect both the transition rules and the density of unoccupied bound states. These unoccupied bound states of the atom are sensitive to charge redistribution from chemical environment including magnetism. There is a need for both theory and experiment on these transitions and on inelastic-scattering cross sections especially near absorption edges. Tabulations of these cross sections for use by the crystallographic community would provide a valuable service for removing the inelastic scattering from the elastic signal of interest. More reliable resonant-dispersion corrections including bound-

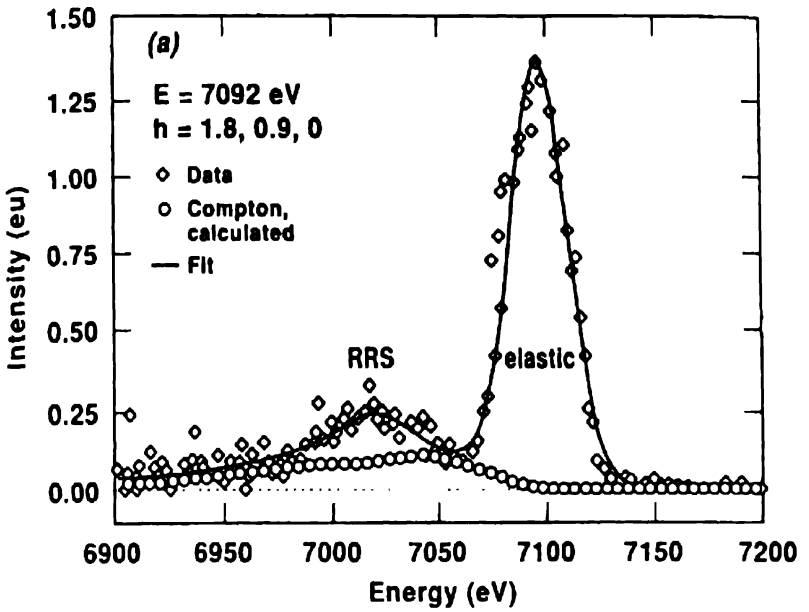


Fig. 10. The Compton scatter ○ is not resolved for this energy resolution of 32 eV while the resonant-Raman (RRS) *K-M* starts at 53 eV below the elastic peak and correspond to the $M_{2,3}$-binding energy.

bound transitions and lifetime broadening to the x-ray atomic scattering factor would also provide more precise phasing information for solutions to complex crystal structures [55]. Shown in Table 3 is a listing of the processes for which tabulated values of the cross sections would be important to the crystallographic community and others.

With the increasing availability of tunable and intense synchrotron radiation sources, experiments with energies from below, through and above the edge are becoming commonplace measurements. Measurements made over a complete energy range of emitted x-rays and electrons including coincident measurements would be of great value in unraveling the primary and secondary mechanisms of absorption and scattering. Polarization and momentum-transfer dependence are required to distinguish between the various possible excitation and de-excitation channels. Comparisons between low and higher atomic-numbered elements where energy levels and shake-up/shake-off probabilities change would be valuable. A more uniform nomenclature would help reduce the confusion for the nonspecialist.

Table 2. Some of the many useful applications of the interaction of x-rays with matter which would benefit from state-of-the-art calculations of the cross sections for the various processes discussed in the text.

**X-RAY INTERACTIONS (1 TO 40 keV): APPLICATIONS AND INFORMATION**

**PHOTOIONIZATION**
- ABSORPTION EDGE SPECTROSCOPY
  - Unfilled Bound States
    - local chemistry
  - EXAFS
    - coordination bond lengths
  - Absorption Cross Sections
  - Radiography-Microscopy - Tomography
- PHOTOELECTRON SPECTROSCOPY
  - Surface Structure
- AUGER SPECTROSCOPY
  - Electronic States
  - Many Body Effects
  - Surfaces
- X-RAY FLUORESCENT SPECTROSCOPY
  - Elemental Analysis and Tomography
  - Energy Levels

**SCATTER**
- ELASTIC (RAYLEIGH)
  - DIFFUSE
    - Coordination, Bond Lengths
    - Short-Range Structures in Crystalline or Amorphous Solids, Liquids, Gases, Defects
    - Macro-microstructures
    - Phonons
  - BRAGG
    - Long Range Periodicity and Defects
    - Thin Films
    - X-Ray Topography
    - Interferometry
    - Chemistry of Site Occupation
- INELASTIC (RAMAN)
  - COMPTON
    - Electron Momentum
    - Inverse Compton
  - RESONANT RAMAN
    - Unfilled Bound States
    - Many Body Effects
  - PLASMON EXCITATIONS
    - Collective Excitations
  - THERMAL MOTION
    - Phonons

Table 3. Improved and easily accessible tabulated cross sections are needed for the following processes to better correct the data and to separate elastic from inelastically scattered x-rays.*

| Process | Tabulated Form |
|---|---|
| Absorption coefficients | $\mu/\rho(E,Z)$ |
| Resonant x ray scattering terms | $f'(E,Z), f''(E,Z)$ |
| Compton<br>Compton-Raman<br>Plasmon | $d\sigma(Z, Ej, Eo, d\Omega, \mathbf{h})$ |
| Resonant Raman | $d\sigma(Z, Ej, Eo, d\Omega, \mathbf{h})$ |
| Bremsstrahlung | $d\sigma(Z, Ej, Eo, d\Omega, \mathbf{h})$ |

*Where appropriate, cross sections need to be tabulated as a function of atomic number $Z$, incident energy $E_j$, energy out $E_0$ solid angle $\Omega$, and momentum transfer $\boldsymbol{h}$.

**Acknowledgments**

The authors express their appreciation to E. D. Specht and F. J. Walker for helpful comments on the manuscript. C. J. Sparks is a research professor at the University of Tennessee, Knoxville and a consultant to the Oak Ridge National Laboratory. This research is sponsored by the Division of Materials Sciences and Division of Chemical Sciences, U.S. Department of Energy under contract DE-AC05-96OR22464 with Lockheed Martin Energy Research Corporation.

**References**

[1] W. C. Röntgen, Ann. Phys. 64, 1 (1898), and discussions in Ref. [24].

[2] W. Friedrich, P. Knipping and M. Laue, Ber. bayer. Akad. Wiss., 303

(1912).

[3] W. L. Bragg, Proc. Camb. Phil. Soc. **17**, 43 (1912).

[4] J. J. Thomson, Phil. Mag. **45**, 172 (1898).

[5] I. Waller, Z. Phys. **51**, 213 (1927).

[6] H. Hönl, Z. Phys. **84**, 11 (1933).

[7] D. H. Templeton, "X-ray resonance, then and now", in *Resonant Anomalous X-Ray Scattering: Theory and Applications*, eds. G. Materlik, C. J. Sparks, and K. Fischer (North-Holland, Amsterdam, 1994) p. 1.

[8] R. W. James, *The Optical Principles of the Diffraction of X-Rays*, Cornell University Press, Ithaca, NY (1948).

[9] H. A. Kramers and R. de L. Kronig (1927) see discussion in Ref. [8].

[10] M. Breinig, M. H. Chen, G. E. Ice, F. Parents, B. Crasemann and G. S. Brown, Phys. Rev. A **22**, 520 (1980).

[11] G. E. Ice, C. J. Sparks, and L. B. Shaffer, in *Resonant Anomalous X-Ray Scattering: Theory and Experiment*, edited by G. Materlik, C. J. Sparks, and K. Fischer (North-Holland, Amsterdam (1994) p. 265.

[12] D. T. Cromer and D. Liberman, J. Chem. Phys. **53** 1891 (1970); Acta Crystallogr. **A37**, 267 (1981).

[13] T. Kawamura and T. Fukamachi, Japan J. Appl. Phys. **17**, Suppl. 17-2, 224 (1978); J. J. Hoyt, D. D. Fontaine and W. K. Warburton, J. Appl. Crystallogr. **17**, 344 (1984).

[14] E. B. Saloman, J. H. Hubbell and J. H. Scofield, At. Data Nucl. Data Tables **38**, 1 (1988).

[15] B. Lengeler, in *Resonant Anomalous X-Ray Scattering: Theory and Applications*, edited by G. Materlik, C. J. Sparks, and K. Fisher (North-Holland, Amsterdam, 1994).

[16] C. T. Chantler, in *Resonant Anomalous X-Ray Scattering: Theory and Applications*, edited by G. Materlik, C. J. Sparks, and K. Fisher (North-Holland, Amsterdam, 1994).

[17] P. Suortti, J. B. Hastings and D. E. Cos, Acta Crystallogr. **A41**, 413 (1985), and references therein.

[18] For detailed discussions of this science see articles in *Resonant Anomalous X-Ray Scattering: Theory and Applications*, edited by G. Materlik, C. J. Sparks, and K. Fisher (North-Holland, Amsterdam, 1994).

[19] W. Kossel, Z. Phys. **2**, 470 (1920); ibid **1**, 119 (1920) and earlier references contained therein.

[20] J. Bergengren, Z. Phys. **3**, 247 (1920).

[21] A. E. Lindh and O. Lundquist, Ark. Math. Astro. och Fysik. 18, Nos. 14, 34, 35 (1924).

[22] A. H. Compton, Bulletin Nat. Res. Council No. 20, 16 (1922); Phys. Rev. **21**, 715 (1923); **22** 409 (1923).

[23] A. Smekal, Naturwissenschaften **11**, 873 (1923).

[24] A. H. Compton, Phys. Rev. **24**, 168 (1924).

[25] B. Davis and D. P. Mitchell, Phys. Rev. **32**, 331 (1928).

[26] A. H. Compton and S. K. Allison, *X-Rays in Theory and Experiment*, (D. Van Nostrand Co., New York, 1935), p. 239.

[27] C. V. Raman, Indian J. Phys. **2**, 387 (1928).

[28] J. W. M. DuMond, Phys. Rev. **33**, 643 (1929).

[29] K. Das Gupta, Phys. Rev. Lett. **3**, 38 (1959).

[30] T. Suzuki, J. Phys. Soc. Japan **22**, 1139 (1967).

[31] T. Suzuki, T. Kishimoto, T. Kaji and T. Suzuki, J. Phys. Soc. Japan. **29**, 730 (1970).

[32] T. Suzuki and H. Nagasawa, J. Phys. Soc. Japan. **39**, 1579 (1975)

[33] A. Pimpale and C. Mande, Pramāna **23**, 279 (1984).

[34] K. Tohji and Y. Udagawa, Phys. Rev. B **36**, 9410 (1987); A. D. Zdetsis and D. K. Papademitriou, Phys. Rev. Lett. **60**, 61 (1988).

[35] G. A. Carlsson, C. A. Carlsson, K. Berggren and R. Ribberfors, Med. Phys. **9**, 868 (1982).

[36] F. Biggs, L. B. Mendelshohn, and J. B. Mann, At. Data Nucl. Data Tables **16**, 201 (1975).

[37] P. Nozieres and D. Pines, Nuono Ciments **9**, 470 (1958).

[38] G. Priftis, A. Theodossiou, and K. Alexopoulos, Phys. Rev. Lett. **27A**, 577 (1968).

[39] W. Schülke, H. Shulte-Shrepping, and J. R. Schmitz, Phys. Rev. B **47**, 12426 (1993).

[40] F. Bloch, Phys. Rev. **48**, 187 (1935).

[41] T. Åberg and J. Utriainen, Phys. Rev. Lett. **22**, 1346 (1969).

[42] T. Åberg and B. Crasemann, in *Resonant Anomalous X-Ray Scattering: Theory and Applications*, edited by G. Materlik, C. J. Sparks, and K. Fisher (North-Holland, Amsterdam, 1994) p. 431.

[43] B. Crasemann, in *Festschrift, Röntgen Centennial*, edited by A. Haase, E. Umbach, and G. Landwehr (Chapman & Hall, New York, in press).

[44] O. Keski-Rahkonen and J. Utriainen, J. Phys. B **7**, 55 (1974).

[45] M. Siegbahn and W. Stenström, Phys. Zeit. **17**, 48 (1916); ibid. 318 (1916).

[46] G. Wentzel, Ann. Phys. **66**, 437 (1921).

[47] R. D. Deslattes, R. E. LaVilla, P. L. Cowan and A. Henins, Phys. Rev. A **27**, 923 (1983).

[48] M. B. Chamberlain, A. F. Burr and R. J. Liefeld, Phys. Rev. A **9**, 663 (1974).

[49] J. K. Lang, Y. Baer and P. A. Cox, J. Phys. F **11**, 121 (1981).

[50] C. J. Sparks, Phys. Rev. Lett. **33**, 262 (1974).

[51] C. J. Sparks, in *Anomalous Scattering*, edited by S. Ramaseshan and S. C. Abrahams (Munksgaard, Copenhagen 1974) p. 175.

[52] Y. B. Bannett and I. Freund, Phys. Rev. Lett. **34**, 372 (1975).

[53] P. Eisenberger, P. M. Platzman and H. Winick, Phys. Rev. Lett., **36**, 623 (1976); Phys. Rev. B., **13**, 2377 (1976).

[54] G. S. Brown, M. H. Chen, B. Crasemann and G. E. Ice, Phys. Rev. Lett. **45**, 1937 (1980).

[55] For a more complete understanding of the crystallographic uses see the conference proceeding of Ref. [18]; a recent conference on the electron and x-ray emission will be published in *Raman Emission by X-Rays*, edited by D. Ederer and J. McGuire (World Scientific Pub. Co., River Edge, NJ, USA, 1996).